Astron. Astrophys. 322, 719–729 (1997)

ASTRONOMY
AND
ASTROPHYSICS

A ROSAT observation of the warm-absorbed soft X-ray spectrum of NGC 4051

Stefanie Komossa and Henner Fink

Max-Planck-Institut für extraterrestrische Physik, D-85740 Garching, Germany

Received 23 July 1996 / Accepted 18 November 1996

Abstract. We present and analyze a pointed ROSAT PSPC observation of the Seyfert galaxy NGC 4051. The X-ray spectrum consists of a powerlaw modified by absorption edges and an additional soft excess during the high-state in source flux. Modeling the spectrum in terms of warm absorption yields a large column density of the ionized material of log $N_{\rm w}$ = 22.7 and an ionization parameter of log U = 0.4. These properties are essentially constant throughout the observation, whereas the luminosity changes by more than a factor of 4. The underlying powerlaw is in its steepest observed state, with a photon index $\Gamma_{\rm x}$ = –2.3. Consulting information from optical observations, evidence for a separate EUV bump component in NGC 4051 is provided. The impact of several parameters on the deduced properties of the ionized material is critically assessed. In particular, the influence of dust mixed with the warm gas is explored and shown to constrain the history or density of the absorber. The absorber-intrinsic optical-UV emission (and absorption) line spectrum is predicted and the possibility of a warm absorber origin of one of the observed emission line regions in NGC 4051 is investigated. Consequences for the narrow-line Seyfert 1 character of NGC 4051 are discussed.

Key words: galaxies: active – individual: NGC 4051 – emission lines – Seyfert – X-rays: galaxies

1. Introduction

NGC 4051 is a spiral galaxy of morphological type SAB with a redshift of z = 0.0023. It hosts a low-luminosity Seyfert 1 nucleus (Seyfert 1943). The object is well known for its rapid X-ray variability which was discovered by Marshall et al. (1983) with the *Einstein* observatory. Subsequently, NGC 4051 has been extensively studied in the X-ray spectral region with all majour X-ray missions (e.g. Lawrence et al. 1985, with *EXOSAT*; Matsuoka et al. 1990, with *Ginga* ; Pounds et al. 1994, with ROSAT ; Mihara et al. 1994, with *ASCA*).

The soft X-ray spectrum of NGC 4051 shows several components. A black-body-like soft excess is seen in source high-states (e.g. Pounds et al. 1994, Mihara et al. 1994). In addition, there is occasional evidence for cold absorption in excess of the Galactic value (Walter et al. 1994). Around 0.8 keV the spectrum exhibits absorption features, interpreted and modeled as the signature of absorption by ionized material along the line of sight (Pounds et al. 1994, with ROSAT survey data; McHardy et al. 1995, with ROSAT PSPC pointed data; Mihara et al. 1994, with *ASCA* data; another study of *ASCA* data by Guainazzi et al. is underway). The existence of a warm absorber in NGC 4051 was firstly proposed by Fiore et al. (1992) as a possible explanation for the observed spectral variability pattern in *Ginga* data. Netzer et al. (1994) found evidence for a warm absorber in NGC 4051 by introducing and applying X-ray colour diagrams.

The overall spectral variability of NGC 4051 is complex with different behaviour at different epochs, and no consistent description of the data has emerged yet. In general, there is a trend for the source to be softer when brighter (Lawrence et al. 1985, Papadakis & Lawrence 1995, with *EXOSAT* data; Matsuoka et al. 1990, with *Ginga* data), traced back by Papadakis & Lawrence (1995) to high flux peaks in the soft (0.05 - 2 keV) energy region only. Matsuoka et al. (1990) favour a correlation of powerlaw index with the 2 - 10 keV luminosity, which Torricelli-Ciamponi & Courvoisier (1995) explain in terms of inverse Compton scattering of thermal UV photons by a population of nonthermal relativistic electrons. Kunieda et al. (1992) and Fiore et al. (1992) describe part or the total of another *Ginga* observation in terms of partial covering of the central source emitting a powerlaw with approximately constant slope.

The optical spectrum of NGC 4051 has been classified as either Seyfert 1.8 (e.g. Rosenblatt et al. 1992) or narrow-line Seyfert 1 (NLSy1 hereafter; e.g. Malkan 1986). The line width (FWHM) of Hβ is 990 km/s (Osterbrock & Shuder 1982), broader than the forbidden lines with a FWHM of [OIII]λ5007 of 330 km/s (De Robertis & Osterbrock 1984). An additional

Send offprint requests to: S. Komossa
(skomossa@mpe-garching.mpg.de)

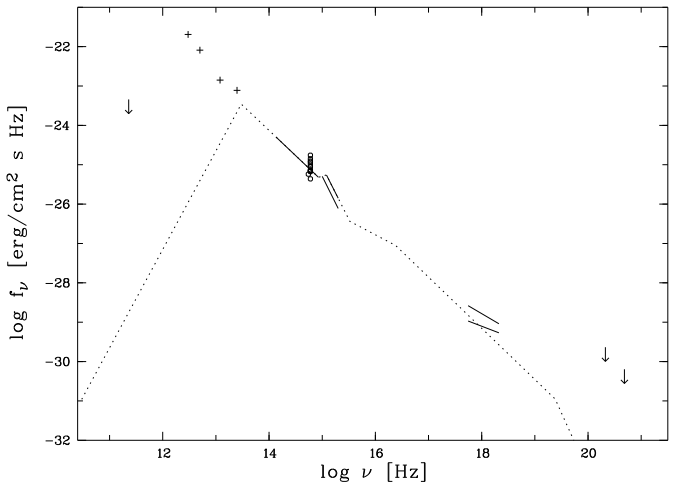

Fig. 1. Extract of the observed spectral energy distribution of NGC 4051 from the radio to the gamma-ray region, compiled from the literature (Edelson et al. 1987, Edelson & Malkan 1986, Done et al. 1990, Malkan 1986, Rosenblatt et al. 1992, Walter et al. 1994, Maisack et al. 1995). Arrows denote upper limits. The circles correspond to measurements of the optical flux at 5000 Å at different epochs (Malkan 1986, Rosenblatt et al. 1992), giving an impression on the amplitude of the optical variability, which is similar in the UV as observed by IUE (Courvoisier & Paltani 1992). The dotted line represents the spectrum chosen for modeling.

weak broad component is seen in Hβ (Veilleux 1991, Rosenblatt et al. 1994). High-ionization coronal lines are present in the optical and IR spectrum, like [FeXI]λ7892 (De Robertis & Osterbrock 1984) and [SiVI]1.96μm (Giannuzzo et al. 1995).

The present X-ray observation was performed with the ROSAT PSPC (Trümper 1983; Pfeffermann et al. 1987) in order to study in detail the warm absorption feature, to discuss the time variability of the spectral components and to assess the possibility of a warm-absorber contribution to one of the emission-line components seen in the IR to UV spectral region.

The paper is organized as follows: In Sect. 2 we present the observations. In Sects. 3 and 4 the spectral and temporal analysis of the data is described and properties of the warm absorber are derived. Sect. 5 is concerned with the discussion of the data; constraints on the unobserved EUV continuum are provided, the properties of the warm gas are discussed and further constrained, the absorber-intrinsic optical-UV emission and absorption is investigated, the influence of dust is assessed, the thermal stability of the warm material is examined, and the NLSy1 character of NGC 4051 is commented on. In Sect. 6 we provide a summary and the conclusions.

A distance of 14 Mpc is adopted for NGC 4051, resulting from a Hubble constant of H_o = 50 km/s/Mpc and the assumption that the galaxy follows the Hubble flow, i.e. any peculiar velocity component is small.

If not stated otherwise, cgs units are used throughout.

2. Data reduction

The observation was performed with the ROSAT PSPC from November 11 – 12, 1993, centered on NGC 4051. The total exposure time is about 12 ksec. The source photons were extracted within a circle chosen to be large enough to ensure that all of the source counts are included, given the detector response to very soft photons which causes an extension of the image below 0.2 keV (Nousek & Lesser 1993). The background was determined by removing all detected sources within the inner field of view. The data were corrected for vignetting and dead-time, using the EXSAS software (Zimmermann et al. 1994). The mean source countrate is about 2.9 cts/s. For the spectral analysis source photons in the amplitude channels 11-240 were binned according to a constant signal/noise ratio of 16σ. For the temporal analysis the minimal binsize in time was 400 s to account for the satellite's wobbling motion.

3. Spectral analysis

3.1. Simple spectral models

A single powerlaw has been previously found to give a poor fit to the X-ray spectrum of NGC 4051. This also holds for the present observation (see Table 1). The resulting powerlaw slope is rather steep, $\Gamma_x \approx -2.9$, and strong residuals remain, with an unacceptable $\chi^2_{\rm red}$ of 3.8. When the cold absorbing column density $N_{\rm H}$ is left as a free parameter, a value slightly higher than the Galactic one is found. For all further fits described below, $N_{\rm H}$ turned out to be either less than or about the same as the Galactic value and thus was fixed to the Galactic column of 0.13 $\times 10^{21}$ cm^{-2} (Elvis et al. 1989; see also McHardy et al. 1995).

Although an improvement of the fit is obtained when adding a soft excess, this model does not provide a satisfactory description of the spectrum, either. Parameterizing the excess component as a black body (with normalization and temperature free) yields $\chi^2_{\rm red}$ = 1.9 with a rather steep underlying powerlaw spectrum (Table 1).

Alternatively, the fit can be improved by adding an absorption edge which is thought to originate from warm gas along the line of sight. With the resulting best fit from a physical warm absorber model (next section) already in mind, the major absorption edges being those of OVII, OVIII and NeX, we modeled the X-ray spectrum with 3 single edges (of the form $\phi(E,\tau) = e^{-\tau(E/E_{\rm edge})^{-3}}$ for $E \geq E_{\rm edge}$) superimposed on a powerlaw. The edge energies were fixed to the theoretical values ($E_{\rm OVII}$ = 0.74 keV, $E_{\rm OVIII}$ = 0.87 keV, $E_{\rm NeX}$ = 1.36 keV) and the optical depths τ left free to vary. We find $\tau_{\rm OVII} = 0.35 \pm 0.15$, $\tau_{\rm OVIII} = 1.1 \pm 0.4$, $\tau_{\rm NeX} = 0.8 \pm 0.4$ and a photon index $\Gamma_x = -2.40 \pm 0.06$.

3.2. Warm absorber models

The spectral absorption structure resulting from a physical absorber is more complex than a simple edge. Assuming the gas to be photoionized by continuum emission of the central pointlike nucleus and assuming it to be in photoionization equilibrium,

Table 1. X-ray spectral fits to NGC 4051 (pl = powerlaw, bb = black body, wa = warm absorber). Model 3 refers to the one with 'standard' assumptions (see text), in model 4 (and only in 4) the data corresponding to the short high-state in source flux (orbit 1) are excluded from the spectral fitting, in model 5 underabundant metals of 0.2 × solar are chosen and in model 6 an IR spectral component as observed by IRAS is added. The errors are quoted at the 95.5% confidence level.

model		log $N_{\rm H}$ [cm^{-2}]	log U	log $N_{\rm w}$ [cm^{-2}]	log Norm$_{\rm pl}$ [ph/cm^2/s/keV]	$\Gamma_{\rm x}$	log Norm$_{\rm bb}$ [ph/cm^2/s]	$kT_{\rm bb}$ [keV]	$\chi^2(d.o.f)$
1	pl	$20.24^{+0.04}_{-0.04}$	-	-	$-2.44^{+0.01}_{-0.01}$ (1)	$-2.92^{+0.07}_{-0.07}$	-	-	230(59)
2	pl + bb	20.11(3)	-	-	$-2.51^{+0.01}_{-0.01}$	$-2.6^{+0.1}_{-0.1}$	$-1.67^{+0.09}_{-0.13}$	$0.10^{+0.01}_{-0.01}$	110(58)
3	wa	20.11	$0.40^{+0.03}_{-0.03}$	$22.67^{+0.02}_{-0.02}$	$-4.49^{+0.01}_{-0.01}$ (2)	–2.3(4)	-	-	67(59)
4	wa, no orb1	20.11	$0.40^{+0.03}_{-0.03}$	$22.67^{+0.02}_{-0.02}$	$-4.52^{+0.01}_{-0.01}$	–2.3	-	-	62(59)
5	wa, met=0.2	20.11	$0.60^{+0.03}_{-0.03}$	$23.38^{+0.02}_{-0.02}$	$-4.49^{+0.01}_{-0.01}$	–2.3	-	-	70(59)
6	wa, IRAS-IR	20.11	$0.20^{+0.03}_{-0.03}$	$22.69^{+0.02}_{-0.02}$	$-4.50^{+0.01}_{-0.01}$	–2.3	-	-	70(59)

(1) Normalization at 1 keV (2) at 10 keV (3) fixed to the Galactic value (4) pre-determined and then fixed (see text)

we calculated a sequence of photoionization models using the code *Cloudy* (Ferland 1993).

The ionization state of the warm absorber can be characterized by the hydrogen column density $N_{\rm w}$ of the warm material and the ionization parameter U, defined as

$$U = Q/(4\pi r^2 n_{\rm H} c) \quad (1)$$

where Q is the number rate of incident photons above the Lyman limit, r is the distance between central source and warm absorber, c is the speed of light, and $n_{\rm H}$ is the hydrogen density (fixed to $10^{9.5}$ cm^{-3} unless noted otherwise). The X-ray absorption structure depends only very weakly on $n_{\rm H}$ ($\approx n_{\rm e}$, where $n_{\rm e}$ is the electron density) and remains unchanged for the range of densities discussed below, given the dominant physical processes; the essential parameter is the column density $N_{\rm w}$. Both quantities, $N_{\rm w}$ and U, are determined from the X-ray spectral fits. Solar abundances (Grevesse & Anders 1989) were adopted if not stated otherwise. We have always assumed the continuum source to be completely covered by the absorber, i.e. no partial covering in which part of the intrinsic X-ray spectrum is seen directly, has been studied. Further, we assume the absorber to be one-component.

The observed spectral energy distribution (SED) of NGC 4051 is shown in Fig. 1. The one chosen for the modeling corresponds to the observed IR to UV spectrum in an intermediate brightness state (corrected for stellar contribution) extrapolated to the Lyman limit, a break at 10μm and an energy index α = –2.5 λ-longwards, an X-ray powerlaw as self-consistently determined from the spectral fitting, and a break into the gamma-ray region at 100 keV.

Data in the NIR to UV spectral region were taken from Done et al. (1990) and are simultaneous but not contemporaneous to the present X-ray observation, although both represent an intermediate brightness state. Anyway, Done et al. (1990) and Hunt et al. (1992) find no short-timescale correlated IR/optical/UV – X-ray variability. Long-term trends are less certain, but Salvati et al. (1993) point to an X-ray high-state contemporaneous with a NIR high-state. The FIR spectrum of NGC 4051 observed by IRAS does not show a turnover shortwards of 100 μm. However, the IRAS points are thought to be contaminated by emission from cold dust of the surrounding galaxy (Edelson & Malkan 1986, Ward et al. 1987) and consequently are not seen by the warm material as a pointlike continuum source. Therefore, the nuclear SED was assumed to break at 10 μm and extend to the radio spectral region with α = –2.5, consistent with the measured millimeter upper limit (Edelson et al. 1987). Anyway, the continuum λ-longwards the Lyman limit usually does not play an important role in determining the ionization state of the warm material and in particular the depth of the X-ray absorption features. (Later we comment on the influence of increased free-free heating, when an IR component as observed by IRAS is added to the nuclear spectrum.) The hard X-ray spectrum was assumed to follow the soft X-ray powerlaw (as was found to be a viable description of the ROSAT –*Ginga* and *ASCA* data; Pounds et al. 1994, Mihara et al. 1994, Guainazzi et al. 1996) and to break at 100 keV, in line with current observations of Seyferts (e.g. Kurfess 1994) and consistent with the observed gamma-ray upper limit (Maisack et al. 1995).

Fitting the warm absorber model to the X-ray spectrum of NGC 4051 results in an ionization parameter of $\log U = 0.40 \pm 0.03$, a warm column density of $\log N_{\rm w} = 22.67 \pm 0.02$, and a photon index of $\Gamma_{\rm x}$ = –2.3 (Table 1). The value of $\Gamma_{\rm x}$ was predetermined in a sequence of fits and then fixed to that value for further modelling (we did not attempt to tune the second digit of $\Gamma_{\rm x}$; a change of $\Delta\Gamma_{\rm x} = +0.1(-0.1)$ results in $\Delta\chi^2 = 24(10)$). Further discussions and conclusions refer to this set of model parameters, if not stated otherwise. The electron temperature T of the warm gas is about 3×10^5 K. There is no evidence for a cold absorbing column larger than the Galactic one. The residuals from the best spectral fit are shown in Fig. 2 and the (unfolded) X-ray spectrum is displayed in Fig. 5. The absorption structure is dominated by highly ionized oxygen (OVIII) and

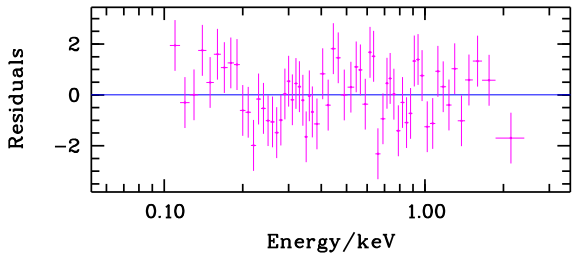

Fig. 2. Residuals of the warm absorber fit to the X-ray spectrum of NGC 4051. The fit parameters are listed in Table 1 and the unfolded spectrum is shown in Fig. 5.

neon. No strong iron edge around 7 keV is predicted (Fig. 5), consistent with higher-energy observations (e.g. Matsuoka et al. 1990). The intrinsic X-ray luminosity (i.e. the one prior to warm absorption) for this model in the 0.1 – 2.4 keV energy range is $L_{\rm x} = 9.5 \times 10^{41}$ erg/s.

Netzer (1993) has discussed the consequences for the X-ray spectral shape of taking into account X-ray emission and reflection by the ionized absorbing gas. For the present observation of NGC 4051 the addition of an emission and reflection component to the X-ray spectrum, calculated with the code *Cloudy* for a covering factor of the warm material of 0.5, only negligibly changes the results ($\log N_{\rm w} = 22.70$) due to the weakness of these components.

The warm absorber fit shown in Fig. 2 shows some residual structure between 0.1 and 0.3 keV. For completeness we note that an additional very soft excess component, parameterized as a black body, removes part of the residuals. Of course, the parameters of such a black body component are not well constrained from X-ray spectral fits. One with $kT_{\rm bb}$ = 13 eV (corresponding to $T_{\rm bb} \approx 150\,000$ K) and an integrated absorption-corrected flux (between the Lyman limit and 2.4 keV) of $F = 7 \times 10^{-11}$ erg/cm^2/s fits the data. It contributes about the same amount to the ionizing luminosity as the powerlaw continuum used for the modeling and has the properties of the EUV spectral component for which evidence is presented in Sect. 5.1.

The observational data were compared to four further model sequences, which consisted of (i) a change in metal abundances of the warm gas up to 0.2 × solar, (ii) the addition of dust with Galactic (ISM) properties to the gas, or a modification of the SED impinging on the absorber, by (iii) the addition of an EUV black body component with a temperature of $T_{\rm bb}$ = 100 000 K or 150 000 K contributing the same amount to the ionizing luminosity as the powerlaw component (the choice of these parameters is motivated and further discussed in Sects. 5.2.1, 5.2.4 and 5.1, respectively), or (iv) the inclusion of a strong IR spectral component as observed by IRAS.

The resulting best-fit model for reduced metal abundances of 1/5 the solar value is given in row 4 of Table 1. The low abundances are mostly reflected in an increase in the corresponding total hydrogen column $N_{\rm w}$, as expected due to the fact that oxygen (and neon) are most important in determining the absorption structure. An additional IR component strongly increases the free-free heating of the gas and the electron temperature rises. An additional black body component in the EUV with the properties given above has negligible influence on the X-ray absorption structure. Dusty models will be further commented on in Sect. 5.2.4.

3.3. Warm absorber plus soft excess ?

The intrinsic, i.e. unabsorbed, powerlaw with index $\Gamma_{\rm x} = -2.3$ is steeper than the Seyfert-1 typical one with –1.9. In fact, fixing the slope of the intrinsic powerlaw to $\Gamma_{\rm x} = -1.9$ (with U and $N_{\rm w}$ as free parameters) leads to a significantly worse fit ($\chi^2{}_{red}$ = 5.2). This still holds when all data points below 0.3 keV (which show some residual structure interpretable as a very soft excess, as mentioned above) are excluded from the spectral fitting ($\chi^2{}_{red} = 4.3$).

Since a soft excess on top of a flat powerlaw might mimick a single steeper powerlaw, we have performed some further tests to check, whether the data can be reconciled with $\Gamma_{\rm x} = -1.9$ plus a soft excess, parameterized as a black body. Firstly, we have fixed the black body temperature to the value found in an *ASCA* observation by Mihara et al. (1994), $kT_{\rm bb}$ = 0.1 keV. In this case, the black body contribution is always found to be negligible (with a normalization of less than 10^{-10} ph/cm^2/s). When the other fit parameters, namely the ionization parameter of the warm absorber, are changed to enforce a black body contribution to the fit, χ^2 remains far above acceptable values. Secondly, $T_{\rm bb}$ was left as an additional free parameter. In this case, a very soft excess is found, with $kT_{\rm bb} \approx 35$ eV, ill-constrained by the ROSAT data, and the overall quality of the fit is not yet acceptable. Systematically steepening the underlying powerlaw, one is lead back to the model presented above, with $\Gamma_{\rm x} = -2.3$. Finally, all data points which correspond to the short *high-state* in source flux and which show some evidence for an additional soft excess ($kT_{\rm bb} \approx 0.12$ keV; detailed in Sect. 4.2) were excluded from the spectral fitting. The underlying powerlaw spectrum remains steep and the deduced parameters of the warm absorber remain unchanged within the error bars (Table 1, model 4).

4. Temporal analysis

4.1. Flux variability

NGC 4051 is known to be rapidly variable. The X-ray light curve of the present observation is shown in Fig. 3. The source is variable by about a factor of 6 within a day. In order to test whether the amplitude of variability is the same in the low and high energy region of the ROSAT band, we have divided the total observed flux in a soft (0.1 keV $\leq E \leq$ 0.5 keV) and a hard (0.5 keV $\leq E \leq$ 2.4 keV) component and normalized each to the mean flux in the corresponding band. (We note that only in this section do we use this 'tight' definition of 'soft' band. Throughout the rest of the paper, the term 'soft excess' more losely refers to a component somewhere in the ROSAT energy band without implying it to be located exclusively below 0.5 keV.) The soft band is dominated by the cold-absorbed powerlaw

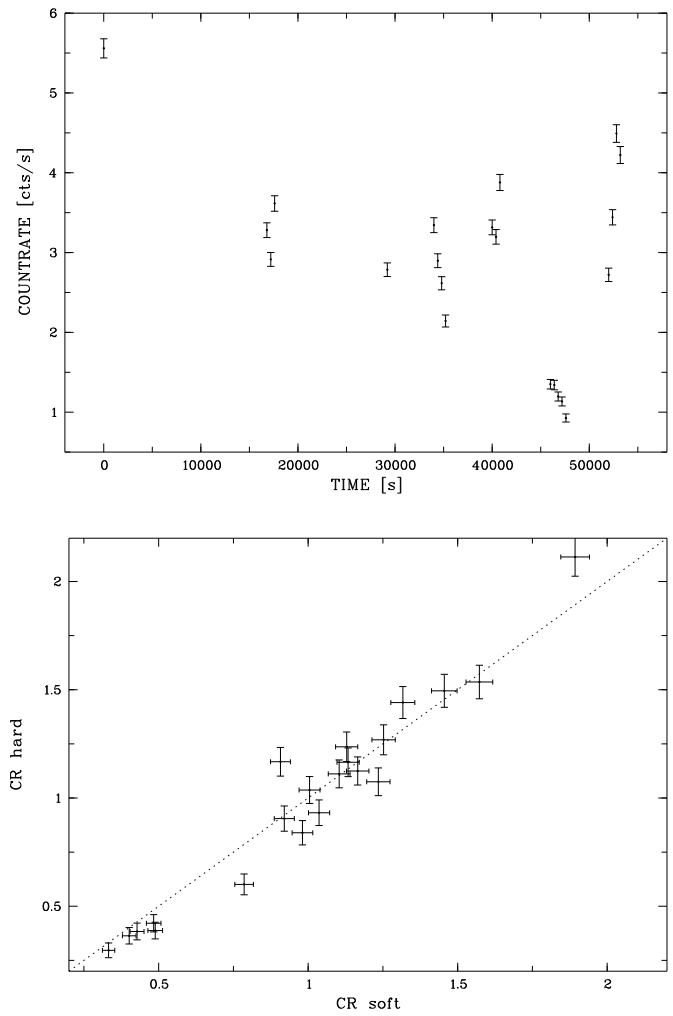

Fig. 3. a X-ray lightcurve of NGC 4051, binned to time intervals of 400 s for the total energy range. **b** Correlation of soft (0.1-0.5 keV) and hard (0.5-2.4 keV) countrate normalized to the mean countrate in the corresponding energy interval. The dotted line represents a linear relation.

component, whereas the dominant feature of the warm absorber, the oxygen absorption edge, is located in the hard band. We find essentially correlated variability between both components (Fig. 3b), although there is a slight trend for the source to be softer when fainter.

4.2. Spectral variability

To check for variability of the warm absorption feature in more detail, we have performed warm-absorber fits to individual subsets of the total observation (referred to as 'orbits' hereafter). The warm column density, $N_{\rm w}$, is not expected to vary on short timescales and was fixed to the value determined for the total observation. The same was done for the unabsorbed powerlaw index $\Gamma_{\rm x}$ = –2.3 (but see comment below). The best-fit ionization parameter turns out to be essentially constant over the whole observation despite strong changes in the intrinsic luminosity (Fig. 4). If the warm material reacted instantaneously to variations in the ionizing luminosity, a clear correlation between U and L would be expected. Given the fact that there are time gaps in the observation and slightly delayed reactions might have escaped observation, one would still expect U to scatter as strongly as L. The constancy of U provides a limit on the density of the warm gas. Its recombination timescale $t_{\rm rec}$ is conservatively estimated from the lack of any reaction of the warm material during the long low-state in orbit 7 (at t = 46 000 – 48 000 s after $t_{\rm start}$; cf. Fig. 3a), resulting in $t_{\rm rec} \gtrsim$ 2000 sec. The upper limit on the density is given by

$$n_{\rm e} \approx \frac{1}{t_{\rm rec}} \; \frac{n_{\rm i}}{n_{\rm i+1}} \; \frac{1}{A}(\frac{T}{10^4})^X \qquad (2)$$

where $n_{\rm i}/n_{\rm i+1}$ is the ion abundance ratio of the metal ions dominating the cooling of the gas and the last term is the corresponding recombination rate coefficient $\alpha^{-1}_{\rm i+1,i}$ (Shull & Van Steenberg 1982 with coefficients A = 6.71 $\times 10^{-11}$, X = 0.726 from Aldrovandi & Pequignot 1973). Oxygen is a major coolant, and given its ionization structure for the best-fit warm absorber model (with an ion abundance ratio of $n_{\rm O^{7+}}/n_{\rm O^{8+}} \approx 0.3$ and a recombination rate coefficient of α = 0.57 $\times 10^{-11}$ cm^3/s) this yields $n_{\rm e} \lesssim 3 \times 10^7 {\rm cm}^{-3}$.

For the above analysis, the intrinsic powerlaw index was fixed to the value derived for the total observation, $\Gamma_{\rm x}$ = –2.3. In fact, when fitting the X-ray spectra of individual orbits, this value always turns out to still represent the best description of the data. Due to the lower number of photons in each orbit, these datasets are less restrictive concerning the values of the fit parameters. However, Fig. 3b already indicates that no strong spectral changes occured, although simultaneous variations of different components that simulate a constant countrate ratio cannot be excluded. To set limits on the variability of $\Gamma_{\rm x}$ within the present observation we have fixed the powerlaw index to –1.9. Re-fitting the low-state (a hardening of the spectrum when the source is less bright would mirror the trend that is observed at higher energies, e.g. Matsuoka et al. 1990), no satisfactory description of the data can be achieved, with a change $\Delta\chi^2$ = 39 as compared to the former best fit.

The spectrum during the first orbit (i.e. the first $\approx$ 800 s) of the total observation, corresponding to a high-state in source flux, shows evidence for an additional black-body-like spectral component with $kT_{\rm bb} \approx$ 0.12 keV and an unabsorbed flux of 7.7 $\times$ 10^{-12} erg/cm^2/s in the ROSAT band, consistent with former observations of a soft excess during source high-states (Pounds et al. 1994, Mihara et al. 1994). If, again, $\Gamma_{\rm x}$ = – 1.9 is enforced, and the parameters of the black body are left free to vary, an additional very soft excess with $kT_{\rm bb} \approx$ 40 eV reproduces the observation. However, a very large column of the warm material is found in this case to compensate the flatter intrinsic powerlaw, log $N_{\rm w}$ = 23.4. If this model applied, a strong change in the column density (by about a factor of 5) during the high-state would have to be invoked, which seems rather unrealistic.

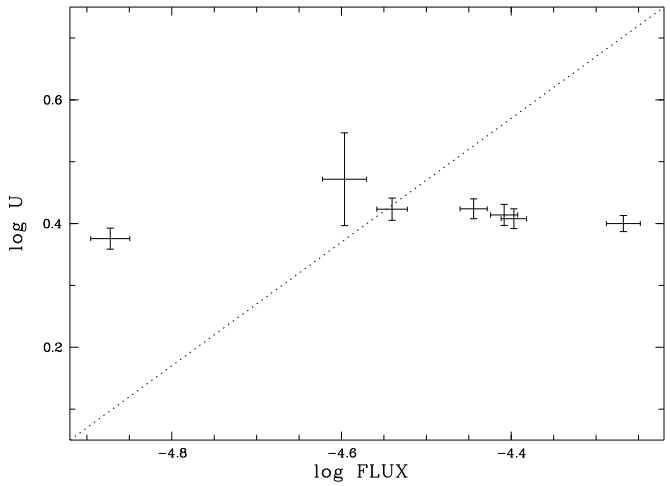

Fig. 4. Ionization parameter U in dependence of the intrinsic X-ray luminosity (parameterized as the powerlaw flux at 10 keV, in photons/cm^2/s/keV), resulting from warm absorber fits to individual orbits of the total observation. The errors correspond to 95.5 % confidence. The dashed line reflects the expected dependence of U on flux if the warm gas reacted immediately to changes in the ionizing luminosity. Within the error bars, U is constant throughout the total observation.

5. Discussion

5.1. SED and ionization parameter

The ionization parameter of the warm absorber, as determined from the X-ray absorption spectrum, is $\log U = 0.4$. Here, the EUV-SED incident on the absorber enters in two ways: (i) by contributing to the total number of photons irradiating the warm gas (Eq. (1)) and (ii) by its influence on the ionization structure of the absorber via its spectral shape. In the following, we discuss constraints on the EUV-SED and the resulting number rate Q of photons above the Lyman limit. It should be noted, however, that the X-ray part of the SED is the one most important in determining the depth of the metal absorption edges, in creating highly ionized ions by K-shell photoionization.

A lower limit on the number of photons in the unobserved EUV-part of the SED is estimated by a powerlaw interpolation between the flux at 0.1 keV (from X-ray spectral fits) and the Lyman-limit (by extrapolating the observed UV spectrum), which was used for the present modeling. This gives $Q = 1.6 \times 10^{52}$ s^{-1}.

Q can also be deduced from the Hβ luminosity. The minimal number of hydrogen-ionizing photons isotropically emitted by the central continuum source is given by the total observed Hβ luminosity. Assuming $T = (10-20) \times 10^3$ K and using Tables. 2.1 and 4.2 of Osterbrock (1989) results in $Q = (2.1-3.8) \times 10^{12}$ $L_{\mathrm{H}\beta}$. The mean observed $L_{\mathrm{H}\beta} = 7.8 \times 10^{39}$ erg/s (Rosenblatt et al. 1992) yields $Q = (1.6 - 2.5) \times 10^{52}$ s^{-1}. It is interesting to note that this is of the same order as the lower limit determined from the assumption of a single powerlaw EUV-SED, suggesting the existence of an additional EUV component in NGC 4051. (Alternatively, it would imply that broad line region (BLR) plus narrow line region (NLR) completely cover the central source (i.e. the covering factor is unity) in contrast to what is observed in the soft X-ray spectrum, i.e. there is no evidence for strong cold absorption in excess of the Galactic value.) However, such an EUV component cannot be identified with the black-body-like soft X-ray excess seen in source high-states (Sect. 4.2; Pounds et al. 1994, Mihara et al. 1994) which turns over already in the soft X-ray region, negligibly contributing to the EUV luminosity. Neither is there a measurable black-body continuum component in the ultraviolet (Edelson & Malkan 1986).

A third approach to Q is via the ionization-parameter-sensitive emission-line ratio [OII]λ3727/[OIII]λ5007 (e.g. Penston et al. 1990). This method makes use of the fact that the [OII]/[OIII] ratio is rather insensitive to the spectral shape of the ionizing continuum (although it tends to overestimate the number of photons, if the emission line region in question contains density inhomogeneities or a large fraction of matter-bounded clouds; Schulz & Komossa 1993). The oxygen ratio, as measured by Malkan (1986) yields an ionization parameter for the NLR of $\log U_{\mathrm{NLR}} = -2.2$ - –2.5. To determine Q, the mean density and distance of the narrow line region have to be known. The density was estimated from the emission line ratio [SII]λ6716/[SII]λ6731 (Veilleux 1991) to be $n_{\mathrm{H}} = 6 \times 10^2$ cm^{-3} and the distance assumed to be $r = 50$ pc (consistent with Schmitt & Kinney 1996), leading to $Q = (1.7-3.4) \times 10^{52}$ s^{-1}.

An additional EUV component may also explain the observational trend that broad emission lines and observed continuum seem to vary independently in NGC 4051 (Osterbrock & Shuder 1982, Peterson et al. 1985, Rosenblatt et al. 1992), as expected if the observed optical-UV continuum variability is not fully representative of the EUV regime.

As noted in Sect. 3.2 there are hints for such an EUV bump in the present X-ray spectrum, although the evidence is rather weak due to the softness of the component. A similar very soft excess, based on much better photon statistics, has been found in the ROSAT spectrum of the narrow-line quasar TON S180 (Fink et al. 1996).

Given the evidence for an EUV bump in NGC 4051 in excess of a simple powerlaw, we have verified that such a component (parameterized as a black body; Sect. 3.2) does not change the fit parameters of the warm absorber within the given error bars except for contributing to U.

An intense IR spectral component, however, leads to a strong heating of the gas and the best-fit ionization parameter decreases somewhat. Underabundant metals (see next section) lead to an increase in the fit value of U. There is approximately a factor of 2 uncertainty in U resulting from this ignorance of continuum shape and chemical composition.

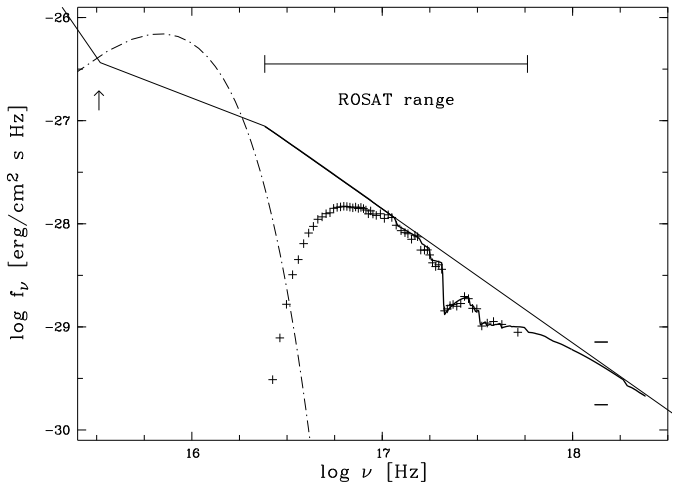

Fig. 5. UV- to X-ray spectrum of NGC 4051. The thin solid line corresponds to the unabsorbed SED chosen for modeling. The thick solid line in the X-ray region shows the best-fit warm-absorbed spectrum corrected for Galactic cold absorption, whereas the crosses correspond to the absorbed spectrum. The dot-dashed line represents the black body with kT = 13 eV that was mentioned in Sect. 3.2. The arrow marks the Lyman limit and the two horizontal bars indicate the amplitude of flux variability when the data are binned to orbits.

5.2. Properties of the warm absorber

5.2.1. Column density and abundances

The warm hydrogen column density of the absorber is log $N_{\rm w}$ = 22.7, adopting solar abundances; an assumption that is usually made. The actual abundances are a priori unknown and might deviate from that by a factor of several. There are indications for underabundant metals in the extended emission line regions of some Seyfert galaxies (e.g. Tadhunter et al. 1989) and in the narrow line regions of Seyfert 2 galaxies by a factor of 1/2 to 1/3 compared to the solar value (Komossa & Schulz 1994). Marshall et al. (1993) constructed a model for the warm electron scattering medium in NGC 1068 (which, in general, might be one component to identify the warm absorber with; and the temperature of which is comparable to that found for the absorber in NGC 4051) with underabundant oxygen of 1/5 $\times$ solar. Depleted gas-phase oxygen abundances are also found by Sternberg et al. (1994) in molecular gas in the central region of NGC 1068, and material evaporating from the torus might be another reservoir for warm absorbing material. X-ray spectral fits do not constrain the abundances. An approach to estimate the chemical composition within the inner region of active galaxies is by emission lines. For the narrow line region, the intensity ratio [OIII]λ4363/[OIII]λ5007 is a good abundance indicator via its temperature sensitivity. Using published emission line intensities of NGC 4051 (Dibai & Pronik 1968, Malkan 1986), we find log [OIII]λ4363/[OIII]λ5007 $\approx$ –0.7, indicative of a rather high temperature and correspondingly low abundances.

Running fits with reduced metal abundances of 1/5 $\times$ solar results in a larger total warm column density, log $N_{\rm w}$ = 23.38, reflecting the fact that the depth of the absorption feature is dominated by oxygen.

5.2.2. Density

The density of the warm gas is not important in determining the X-ray spectral shape at a fixed time. A limit was drawn from the variability behaviour (Sect. 4.2), which resulted in $n_{\rm H} \lesssim 3 \times 10^7 {\rm cm}^{-3}$. We come back to this point in Sect. 5.3.1.

With $n_{\rm H} \leq 3 \times 10^7 {\rm cm}^{-3}$, the thickness of the warm absorber is $D \geq 2 \times 10^{15}$ cm.

5.2.3. Location

The location of the warm material is poorly constrained from X-ray spectral fits alone. The absorber might be part of the broad line region or situated farther outwards, e.g. in the narrow line region. The emission line contribution of an optically thin matter-bounded BLR component in active galaxies was discussed by Shields et al. (1995), who also particularly pointed out that this gas might act as an X-ray warm absorber.

Using $Q = 1.6 \times 10^{52}$ s^{-1} as derived from the powerlaw description of the EUV spectrum and the upper limit of the density of the warm gas as determined from the X-ray variability results in a distance of the absorber from the central power source of $r \geq 3 \times 10^{16}$ cm. Conclusive results for the distance of the BLR in NGC 4051 from reverberation mapping, that would allow a judgement of the relative positions of both components, do not yet exist: Rosenblatt et al. (1992) find the optical continuum to be variable with large amplitude, but no significant change in the Hβ flux.

5.2.4. Influence of dust

Dust might be expected to survive in the warm absorber, e.g. depending on its distance from the central energy source. A rough estimate for the evaporation distance $r_{\rm ev}$ of dust is provided by $r_{\rm ev} \approx \sqrt{L_{46}}$ pc, where L is the integrated continuum luminosity in 10^{46} erg/s (Netzer 1990), leading to $r_{\rm ev} \approx 0.02$ pc for NGC 4051.

Mixing dust of Galactic ISM properties (including both, graphite and astronomical silicate; Ferland 1993) with the warm gas in NGC 4051 and self-consistently re-calculating the models leads to maximum dust temperatures of 2200 K (graphite) and 3100 K (silicate), above the evaporation temperatures (for a density of $n_{\rm H} = 5 \times 10^7$ cm^{-3} and U, $N_{\rm w}$ of the former best-fit model; Sect. 3.2). For $n_{\rm H} \lesssim 10^6$ cm^{-3}, dust can survive throughout the absorber. However, it strongly changes the equilibrium conditions and ionization structure of the gas via strong photoelectric heating and collisional cooling. For relatively high ionization parameters, dust very effectively competes with the gas in the absorption of photons (e.g. Laor & Draine 1993).

An interesting point to pursue in this context is the following: An old puzzle is the lack of any transition region between BLR and NLR (judged from missing 'intermediate' line emission). Netzer & Laor (1993) proposed this to be due to the relatively

more important influence of dust in an intermediate zone. Can the warm absorber be identified with this transition region ?

Firstly, re-running a large number of models, we find no successful fit of the X-ray spectrum. This can be traced back to the relatively higher importance of edges from more lowly ionized species, significantly changing the X-ray absorption spectrum and particularly a very strong Carbon edge. Secondly, independent evidence for non-dusty warm gas comes from the observed UV and EUV spectrum, if these components travel along the same path as the X-ray spectrum. The 2175 Å bump in the UV spectrum of NGC 4051 is not particularly strong (e.g. Walter et al. 1994) and NGC 4051 is detected by EUVE (Marshall et al. 1995). (There are various possibilities to change the properties of dust mixed with the warm material. The one which minimizes the aforementioned observable features, i.e. weakens the 2175 Å absorption and the 10μ IR silicon feature, and is UV gray, consists of a modified grain size distribution, with a dominance of larger grains (Laor & Draine 1993). However, again, such models do not fit the observed X-ray spectrum, even if silicate only is assumed to avoid a strong carbon feature and its abundance is depleted by 1/10.) Indubitably, the dust in NGC 4051 could be significantly different from the Galactic one. However, too many additional free parameters are introduced in this case to warrant a more detailed study.

We conclude that the soft X-ray spectrum of NGC 4051 is not dominated by a (Galactic-ISM-like)*dusty* warm absorber. We emphasize, however, that dusty warm absorbers might explain the low-energy absorption edges seen in some active galaxies (work in progress, for first results see Komossa & Fink 1996).

The absence of dust in the warm material would imply either (i) the *history* of the warm gas is such that dust was never able to form, like e.g. in an inner-disc driven outflow (e.g. Königl & Kartje 1994, Murray et al. 1995, Witt et al. subm.) or (ii) if dust originally existed in the absorber, the *conditions in* the gas have to be such that dust destruction is guaranteed. In the latter case, one obtains an important constraint on the density (location) of the warm gas, which then has to be high enough (near enough) to ensure the dust is destroyed. For the present case (and Galactic-ISM-like dust) only a narrow range in density around $n_{\rm H} \approx 5 \times 10^7$ cm^{-3} is allowed. For lower densities, dust can survive in at least part of the absorber and higher densities have already been excluded in Sect. 4.2.

5.2.5. Warm-absorber intrinsic line emission and covering factor

Constraints on the covering factor of the warm gas result from (i) its emissivity in emission lines, which has to be low enough not to predict line emission stronger than the observed one, and (ii) the desire to account for the rather large number of Seyferts which show evidence for warm absorption (e.g. Fabian 1996), leading to the expectation of a correspondingly large *mean* covering.

In particular, it is interesting to ask whether one of the emission line regions present in NGC 4051 (and in Seyfert galaxies in general), like the coronal line region, or the one responsible for the broad component seen in Hβ in NGC 4051, can be identified with the warm absorber.

In the case of NGC 4051, the maximal warm-absorber intrinsic Hβ emission predicted for the best-fit model is only about 1/220 of the observed $L_{\rm H\beta}$. Rescaling the strongest predicted optical emission line, [FeXIV]λ5303, correspondingly leads to an intensity ratio [FeXIV]$_{\rm wa}$/H$\beta_{\rm obs} \approx 0.01$. This compares to the observed upper limit of [FeXIV]/H$\beta \lesssim 0.1$ as estimated from a spectrum by Peterson et al. (1985) and it is consistent with a covering of the warm material of less or equal 100%.

Due to the low emissivity of the warm gas, no strong UV - EUV emission lines are produced (e.g. HeII $\lambda1640_{\rm wa}$/H$\beta_{\rm obs} \leq$ 0.06, NeVIII $\lambda774_{\rm wa}$/H$\beta_{\rm obs} \leq$ 0.2, FeXVI $\lambda343_{\rm wa}$/H$\beta_{\rm obs} \leq$ 2.0).

Consequently, no known emission line component in NGC 4051 can be fully identified with the warm absorber.

This conclusion still holds when the properties of the warm material are changed compared to the 'standard' assumptions (but note, that only one parameter is varied at a time): The strength of e.g. [FeXIV] is also dependent on the density and changes by a factor of several depending on the value of $n_{\rm H}$, but stays below the observed upper limit. For subsolar metal abundances of the absorber HeII λ1640 becomes the strongest line in the UV-optical region due to the increased helium column necessary to ensure the same column in metal ions and thereby the same strength of the absorption edges in X-rays. For metal abundances of 0.2 $\times$ solar, we find HeII $\lambda1640_{\rm wa}$/H$\beta_{\rm obs} \leq 0.35$. A strong additional IR spectral component incident on the warm gas slightly influences the line emission, although again, there is no strong contribution to the optical-UV spectrum.

5.2.6. UV absorption lines

The ionization structure of the best-fit warm absorber model indicates that the expected UV absorption by e.g. C^{3+} or N^{4+} is low. A common UV - X-ray absorber has been found in some active galaxies by Mathur and collaborators (e.g. Mathur 1994). In the following we give the expected equivalent widths for the UV lines CIV λ1549, NV λ1240 and Lyα predicted by the warm absorber model. The column density in C^{3+} is $\log N_{\rm C^{3+}} = 13.45$ which yields $N_{\rm C^{3+}} \lambda f = 10^{8.09}$ cm^{-1}, where $\lambda = 1549$ Å and $f = 0.28$ is the oscillator strength for CIV (Allen 1955). Performing a standard curve of growth analysis (Spitzer 1978) this evaluates to give an equivalent width of $\log W_\lambda/\lambda = -4.02^{+0.05}_{-0.08}$ where the uncertainties refer to values of the velocity spread parameter b = 100 km/s (for '+') and 20 km/s (for '–') whereas the central value is calculated with b = 60 km/s. Correspondingly, we find for NV λ1240 $\log N_{\rm N^{4+}} = 12.90$ and $\log W_\lambda/\lambda = -4.69$ and for Lyα $\log N_{\rm H^0} = 15.94$ and $\log W_\lambda/\lambda = -3.04^{+0.20}_{-0.44}$. HST spectra would allow to search for these absorption lines and thereby further constrain the properties of the warm material.

5.3. Time variability of the spectral components and comparison with other observations

5.3.1. Warm absorber

In the preceding discussion, photoionization equilibrium was assumed. That photoionization indeed plays an important role for the ionization of warm material is shown by a direct reaction of the absorber (i.e. the depth of the OVIII absorption edge) in MCG-6-30-15 to changes in the continuum (Otani et al. 1996). The equilibrium state of the gas depends on its reaction timescale compared to the timescale of changes in the continuum flux (see Krolik & Kriss 1995). In case the continuum variations are slow compared to the recombination timescale, the warm material re-adjusts to each continuum level, whereas a mean continuum is appropriate for modeling in the opposite case. The latter seems to apply to the present observation, with no reaction of the warm gas despite changes in the luminosity. However, in the long term there are changes in the ionization parameter of the gas: An earlier ROSAT observation shows both, lower mean luminosity and ionization parameter (McHardy et al. 1995; treating and re-fitting these data with the same data reduction procedures and model assumptions as carried out for the present observation yields $\log U = 0.2, \log N_{\rm w} = 22.45, \Gamma_{\rm x} = -2.2$ and an integrated (0.1-2.4 keV) luminosity of $L_{\rm x} = 5.4 \times 10^{41}$ erg/s). Although this might mean that the warm material follows long term trends in the luminosity but not the very short-time variability, the situation seems to be more complex. McHardy et al. (1995) and Guainazzi et al. (1996) find U to be variable within one day. McHardy et al. interpret an increase in U in two orbits as a time-delayed reaction of the absorber to a continuum high-state. The limit on the density of the ionized material estimated by Guainazzi et al. is $n_{\rm H} \geq 10^7$ cm^{-3}. (Note an uncertainty in the density estimate of a factor of several resulting from e.g. the exact values chosen for the temperature of the warm gas, the ion abundance ratio, and the estimated time interval.) Comparing these observations with the present one, the implications are either (i) time gaps just prevented observing a reaction of the warm gas within the current data, or (ii) the warm material does not see the luminosity changes in the present observation, or (iii) the density of the warm gas varies with time, or (iv) the ionization state of the absorber is not dominated by photoionization (see Krolik & Kriss 1995, Reynolds & Fabian 1995 for some alternatives). None of the possibilities can be decided upon with the present data, but we note the following:

Possibility (i) would nearly pin down the density of the warm absorber, to lie in a narrow range around 10^7 cm^{-3}.

(ii) A scenario in which the warm gas does not see luminosity changes is one in which the variability is not intrinsic to the central continuum source but caused between the absorber and the observer. Wachter et al. (1988) proposed the existence of fast moving, dense blobs of matter within the inner region of active galaxies, partially blocking the line of sight to the continuum source. A similar scenario was invoked by Kunieda et al. (1992) to explain different flux states seen in a *Ginga* observation of NGC 4051. The present observation is consistent with the blob model, if the source were in state 'C' (in the terminology of Kunieda et al., referring to variable soft and constant hard observed flux). We lack simultaneous observations in the harder X-ray region but placing blobs with a column density of $N_{\rm H} \approx 10^{24.3}$ cm^{-2}, as proposed by Kunieda et al., along the line of sight would completely absorb the incident radiation in the ROSAT sensitivity range. In that case, no density constraint on the warm material could be derived. But the origin of the blobs and their fast movement (the latter in combination with their large number to account for the observed flux states) remain to be solved.

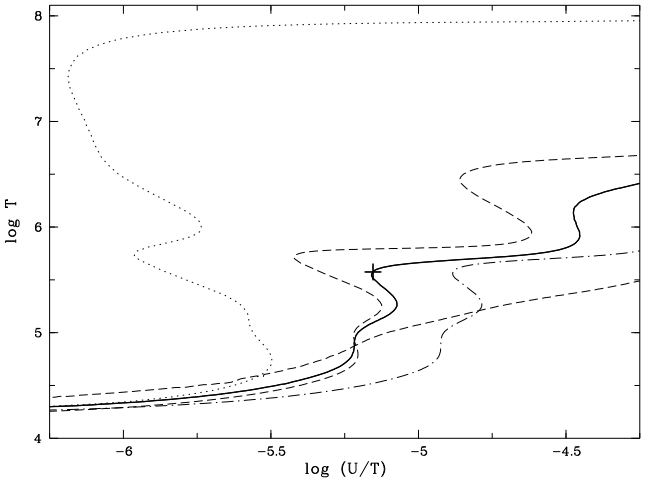

Fig. 6. Equilibrium gas temperature T against U/T for various SEDs incident on the gas and abundances of the gas. The solid line corresponds to the SED of NGC 4051 used for the modeling. The position of the warm absorber is marked. The other models correspond to a modification of either metal abundances of 0.2 × solar (lower dashed line) or 3 × solar (upper dashed line) or spectral shape; dot-dashed: additional EUV black body component as described in Sect. 3.2, dotted: 'mean Seyfert' continuum but with $\Gamma_{\rm x} = -1.5$, for comparison.

(iii) Time-dependent density occurs e.g. if the absorber is in the form of an expanding cloud or consists of inhomogeneous material e.g. in orbital motion. In the latter case variability of the observed warm column density is also expected, which indeed is observed. There is approximately a factor of 2 change in warm column between the two ROSAT observations, being separated by 2 years (Nov. '91 and Nov. '93), and a factor of larger than 10 compared to the *ASCA* data (April '93) of Mihara et al. (1994), who derived $\log N_{\rm w} = 21.3 \pm 0.2$. Guainazzi et al. (1996) find for a second *ASCA* observation (July '94) roughly $\log N_{\rm w} \approx 22.3$, and indications for variability in the OVII edge.

In this context, it is also interesting to note that the warm gas in NGC 4051 is located near an instable region in the $U/T - T$ diagram. A possible 3 phase equilibrium of the ionized absorber in MCG-6-30-15 was discussed by Reynolds & Fabian (1995). The results of a similar analysis for NGC 4051 are shown in Fig. 6. Those regions of the equilibrium curve in which the temperature T is multi-valued for constant U/T, i.e. pressure, allow for the existence of multiple phases in pressure balance. The parts with negative gradient correspond to thermally unstable

equilibria. For comparison, the corresponding curves for metal abundances deviating from the solar value are shown.

5.3.2. Powerlaw component

The possibility of producing all observed *spectral* variability in NGC 4051 by warm absorption has been repeatedly mentioned (e.g. Matsuoka et al. 1990, Fiore et al. 1992, Mc Hardy et al. 1995). We find a significantly steeper powerlaw slope (Γ_x = –2.3) as compared to other observations (e.g. Γ_x = –1.88, Mihara et al. 1994). Consequently, not all soft X-ray spectral variability in NGC 4051 can be traced back to the influence of the warm absorber. In particular, the powerlaw slope is also steeper than is predicted by currently popular non-thermal pair models (e.g. Svensson 1994).

Short-timescale variability of Γ_x during one *Ginga* observation has been favoured by Matsuoka et al. (1990; and has recently been found in *ASCA* data, Guainazzi et al. 1996). In the *Ginga* data, when described by a powerlaw SED, a change of the 2–10 keV flux by a factor of 3–4 was accompanied by a change $\Delta\Gamma_x$ = 0.4–0.5. During the present observation, we find Γ_x to be essentially constant despite changes in flux by a factor of larger than 4. This corroborates the complex and probably time-dependent behaviour of this source.

5.4. NLSy1 - character of NGC 4051

NLSy1 galaxies generally exhibit steep soft X-ray spectra and narrow Balmer lines (see Boller et al. 1996 for a recent detailed discussion). These properties are also shown by NGC 4051, in the sense that a simple powerlaw fit to the X-ray spectrum results in a rather steep powerlaw with Γ_x = –2.9 and the FWHM of Hβ is less than 1000 km/s. However, much of the X-ray spectral steepness of NGC 4051 is caused by the presence of the warm absorber. On the other hand, the intrinsic powerlaw slope is still steeper than the canonical one with Γ_x = –1.9. And an additional soft excess is seen in source high-states. This points to the complexity of NLSy1 spectra with probably more than one mechanism at work to cause the X-ray spectral steepness.

A *dusty* environment in NLSy1 galaxies was proposed as one explanation for the narrowness of their broad lines (Goodrich 1989). Dusty *warm* gas was suggested to exist in the infrared loud quasar IRAS 13349+2438, which has several properties in common with NLSy1 galaxies (Brandt et al. 1996). In case of NGC 4051 no successful description of the X-ray spectrum is achieved when compared to models including dust. The general trend holds that it is more difficult to produce steep soft X-ray spectra with dusty absorbers. On the contrary, the existence of relatively stronger absorption edges from more lowly ionized species generally leads to an effective *flattening* of the spectrum when the edges are not individually resolved.

6. Summary and conclusions

We detect the following spectral components in the Nov. 1993 spectrum of NGC 4051: A powerlaw in its steepest observed state with Γ_x = –2.3, modified by the presence of a warm absorber, and evidence for a black-body-like soft excess during the flux high-state with $kT_{bb} \approx 0.1$ keV. The first two components are essentially constant during the observation, but significantly variable when compared to former observations. Mainly arguments on the number Q of ionizing photons and optical emission line ratios hint to a further bump component in the EUV.

The warm absorber component has been modeled in more detail, which yields a column density of $\log N_w$ = 22.7 and an ionization parameter of $\log U$ = 0.4 (from X-ray spectral fits), a limit on the density of $n_H \lesssim 3 \times 10^7 \mathrm{cm}^{-3}$ (from variability arguments) translating into a distance from the nucleus of $r \gtrsim 3 \times 10^{16}$ cm, and a covering that can be as large as 100 % (from emission line arguments). Observational evidence (no indications of strong reddening along the line of sight, e.g. from the UV spectrum) and model results (no successful X-ray fit) strongly suggest the absorber to be dust free.

Observable consequences of the existence of the ionized material in other spectral regions (in the form of emission or absorption lines) are found to be small: None of the observed emission line regions in NGC 4051 can be fully identified with the warm absorber. The possibility of a contribution to observed individual lines (that would complicate line intensity modeling or reverberation mapping), namely to HeII λ1640, remains in case of subsolar metal abundances of the absorber.

Acknowledgements. The ROSAT project is supported by the German Bundesministerium für Bildung und Wissenschaft (BMBW/DARA) and the Max-Planck-Society. We are indepted to Gary Ferland for providing *Cloudy*. This research has made use of the NASA/IPAC extragalactic database (NED) which is operated by the Jet Propulsion Laboratory, Caltech, under contract with the National Aeronautics and Space Administration.

References

Aldrovandi S.M., Pequignot D., 1973, A&A 25, 137
Allen C. W., 1955, *Astrophysical Quantities*, University of London: Athlone Press
Boller Th., Brandt W.N., Fink H.H., 1996, A&A 305, 53
Brandt W.N., Fabian, A.C., Pounds K.A., 1996, MNRAS 278, 326
Courvoisier T. J., Paltani S., 1992, *IUE-ULDA access guide 4*
De Robertis M.M., Osterbrock D.E., 1984, ApJ 286, 171
Dibai E.A., Pronik V.I., 1968, Sov. Astr. 11 , 767
Done C., Ward M. J., Fabian A.C., et al., 1990, MNRAS 243, 713
Edelson R.A., Malkan M.A., 1986, ApJ 308, 59
Edelson R.A., Malkan M.A., Rieke G.H., 1987, ApJ 321, 233
Elvis M., Lockman F.J., Wilkes B.J., 1989, AJ 97, 777
Fabian A.C., 1996, MPE Report 263, H.U. Zimmermann, J. Trümper, H. Yorke (eds.), 403
Ferland G.J., 1993, University of Kentucky, Physics Department, Internal Report
Fink H.H., Walter R., Schartel N., Engels D., 1996, A&A, in press
Fiore F., Perola G.C., Matsuoka M., Yamauchi M., Piro L., 1992, A&A 262, 37
Giannuzzo E., Rieke G.H., Rieke M.J., 1995, ApJ 446, L5
Goodrich R.W., 1989, ApJ 342, 224
Grevesse N., Anders E., 1989, in Cosmic Abundances of Matter, AIP 183, ed. C.J. Waddington, New York: American Institute of Physics

Guainazzi M., Mihara T., Otani C., Matsuoka M., PASJ, submitted
Hunt L.K., Mannucci F., Salvati M., Stanga R.M., 1992, A&A 257, 434
Komossa S., Schulz H., 1994, in *The Analysis of Emission Lines* (STScI Symp. contributed papers), R.E. Williams, M. Livio (eds.), 30
Komossa S., Fink H., 1996, in *Emission Lines in Active Galaxies: New Methods and Techniques*, B.M. Peterson, F.-Z. Cheng, and A.S. Wilson (eds.), in press
Königl A., Kartje J.F., 1994, ApJ 434, 446
Krolik J.H., Kriss G.A., 1995, ApJ 447, 512
Kunieda H., Hayakawa S., Tawara Y., et al., 1992, ApJ 384, 482
Kurfess J.D., 1994, in *AGN across the Electromagnetic Spectrum* (IAU Symp. 159), T.J.-L. Courvoisier & A. Blecha (eds.), 39
Laor A., Draine B.T., 1993, ApJ 402, 441
Lawrence A., Watson M.G., Pounds K.A., Elvis M., 1985, MNRAS 217, 685
Maisack M., Collmar W., Barr P., et al., 1995, A&A 298, 400
Malkan M., 1986, ApJ 310, 679
Marshall F.E., Holt S.S., Mushotzky R.F., Becker R.H., 1983, ApJ 269, L31
Marshall F.E., Netzer H., Arnaud K.A., et al., 1993, ApJ 405, 168
Marshall H.L., Fruscione A., Carone T.E., 1995, ApJ 439, 90
Mathur S., 1994, ApJ 431, L75
Matsuoka M., Piro L., Yamauchi M., Murakami T., 1990, ApJ 361, 440
McHardy I.M., Green A.R., Done C., et al., 1995, MNRAS 273, 549
Mihara T., Matsuoka M., Mushotzky R., et al., 1994, PASJ 46, L137
Murray N., Chiang J., Grossman S.A., Voit G.M., 1995, ApJ 451, 498
Netzer H., 1990, in Saas-Fee Lecture Notes 20, T.J.-L. Courvoisier and M. Mayor (eds.)
Netzer H., 1993, ApJ 411, 594
Netzer H., Laor A., 1993, ApJ 404, L51
Netzer H., Turner T.J., George I.M., 1994, ApJ 435, 106
Nousek J., Lesser A., 1993, ROSAT Newsletter 8, 13
Osterbrock D.E., 1989, *Astrophysics of Gaseous Nebulae and Active Galactic Nuclei*, Univ. Sci. Books: Mill Valley
Osterbrock D.E., Shuder J.M., 1982, ApJS 49, 149
Otani C., Kii T., Reynolds C. S., et al., 1996, PASJ 48, 211
Papadakis I.E., Lawrence A., 1995, MNRAS 272, 161
Penston M.V., Robinson A., Alloin D., et al., 1990, A&A 236, 53
Peterson B.M., Crenshaw D.M., Meyers K.A., 1985, ApJ 298, 283
Pfeffermann E., Briel U.G., Hippmann H., et al., 1987, SPIE 733, 519
Pounds K.A., Nandra K., Fink H., Makino F., 1994, MNRAS 267, 193
Reynolds C.S., Fabian, A.C., 1995, MNRAS 273, 1167
Rosenblatt E.I., Malkan M.A., Sargent W.L.W., Readhead A.C.S., 1992, ApJS 81, 59
Rosenblatt E.I., Malkan M.A., Sargent W.L.W., Readhead A.C.S., 1994, ApJS 93, 73
Salvati M., Hunt K.L., Calamai G., et al., 1993, A&A 274, 174
Schmitt H. R., Kinney A. L., 1996, ApJ, in press
Schulz H., Komossa S., 1993, A&A 278, 29
Seyfert C. K., 1943, ApJ 97, 28
Shields J.C., Ferland G.J., Peterson B.M., 1995, ApJ 441, 507
Shull J.M., Van Steenberg M., 1982, ApJS 48, 95 & ApJS 49, 351
Spitzer L., 1978, *Physical Processes in the Interstellar Medium*
Sternberg A., Genzel R., Tacconi L., 1994, ApJ 436, L131
Svensson R., 1994, ApJS 92, 585
Tadhunter C.N., Robinson A., Morganti R., 1989, ESO conf. proc. 32, R.A.E. Fosbury, E.A.J. Meurs (eds.), 293
Torricelli-Ciamponi G., Courvoisier T.J.-L., 1995, A&A 296, 651
Trümper J., 1983, Adv. Space Res. 2, 241
Veilleux S., 1991, ApJ 369, 331
Wachter K.W., Strauss M.A., Filippenko A.V., 1988, ApJ 330, 91
Walter R., Orr A., Courvoisier T.J.-L., et al., 1994, A&A 285, 119
Ward M., Elvis M., Fabbiano G., et al., 1987, ApJ 315, 74
Witt H.J., Czerny B., Zycki P.T., MNRAS, submitted
Zimmermann H.U., Becker W., Belloni T., et al., 1994, MPE report 257

This article was processed by the author using Springer-Verlag LaTeX A&A style file *L-AA* version 3.